

A Computational Study of the End Gas Autoignition and Shock Development by Flame Front and Local Hot Spot

Aliou Sow ^a, Bok Jik Lee ^b and Hong G. Im ^a

^a Clean Combustion Research Center, King Abdullah University of Science and Technology (KAUST)
Thuwal, Saudi Arabia

^b Gwangju Institute of Science and Technology (GIST)
Gwangju, South Korea

1 Introduction

Towards higher efficiencies and lower emissions, modern internal combustion (IC) engines are downsized and designed to operate in boosted conditions using direct fuel injection to achieve higher compression ratio. A critical engineering challenge in such engines is its propensity to develop knock. Due to the increased chamber pressure, the end gas ahead of the propagating flame may autoignite as the pressure continues to increase through the compression stroke and flame growth. In an excessive case, this can lead to a super-knock event, causing severe damages on the engine. Considerable efforts have been made in order to understand the end gas autoignition characteristics and super-knock event [1–4]. Since the seminal work by Zeldovich [5] on the general characterization of ignition modes, Bradley and coworkers [6–10] investigated the effects of the initial temperature gradients on the propagation modes, and proposed a diagram to identify the occurrence of detonation in terms of key parameters. In [11], It was observed that, depending on the initial pressure, the initial temperature, and the chamber length, three different end gas combustion modes emerge: normal flame propagation without autoignition, autoignition without detonation development, and detonation. It was also reported that higher reactivity of the end gas as well as larger combustion chamber promote autoignition and detonation development. Flame acceleration and transition to detonation was also observed in [8, 11]. More recently, Chen and coworkers [12] extended 1D computational studies to consider complex fuels, and the effects of nonuniform concentration field were subsequently investigated [13]. Building on these existing studies, the present paper aims to provide further insights into the interaction between the flame front and local hot spot, and its impact on the subsequent shock/detonation development. One-dimensional high fidelity simulations were conducted with accurate shock-capturing schemes based on WENO algorithms [14].

2 Mathematical and Numerical Models

A reactive stoichiometric hydrogen-air mixture was used in our calculations. One-dimensional compressible Navier-Stokes and species conservation equations were solved computationally. The chemical mechanism for hydrogen/air mixtures involved 9 reactive species and 23 elementary reaction steps, validated at high pressure conditions [15]. The computational configuration is similar to that in [11], which is a one-dimensional closed chamber with impermeable and adiabatic walls at both boundaries. The combustion chamber length was set to 4 cm. For the initial condition, the Cantera [16] solution for a freely-propagating premixed hydrogen-air flame with detailed transport properties was mapped within 0.5 cm at the left wall to ignite the flame. The developing flame, herein referred to as the leading flame, propagates to the right where the initial pressure and velocity are initially homogeneous. In addition, a localized hot spot with a width of 0.5 cm was initiated at a distance of 2 cm. The peak temperature of the hot spot was 100 K higher than the bulk gas, and decreased linearly with the distance x . Non-uniformity of active radicals was not considered in these calculations.

For the numerical procedure, a 5th order shock-capturing WENO scheme is used for the convective part. For the viscous components, a high-fidelity finite difference method using 8th order central difference was employed. To advance the solution in time, a 3th order explicit Runge-Kutta scheme was used. To capture the interaction between pressure waves and chemical reaction a uniform grid spacing of 4 microns was chosen.

3 Results and Discussion

We first consider a flame propagating in a quiescent mixture with a initial temperature of $T_0 = 1100$ K and a initial pressure of $P_0 = 10$ atm. Fig. 1 depicts the distributions of temperature, pressure, velocity and H_2 mass fraction at different instants. At $163.7 \mu\text{s}$, the deflagration front travels a distance of approximately 10.1 mm with a mean velocity of 61.7 m/s. Meanwhile, the temperature increases due to the chemical heat released via a thermal explosion (see Fig. 1 (d)). A pressure increase is also noted from 10 to approximately 12 atm. At $195.6 \mu\text{s}$ the end gas spontaneously ignites at the right adiabatic wall. The autoignition of end gas is the consequence of the pressure waves emanating from the propagating flame that continuously compress the fresh mixture near the right wall. The autoignitive front, created near the wall, propagates towards the leading flame. The unburned gases trapped between the main propagating flame and the autoignitive front are driven to higher and higher compression due to the combine effects of both reacting fronts. Note that the autoignitive front propagates at a much higher speed compared to the deflagration front on the left, suggesting that it is in the spontaneous ignition regime [5, 17, 18]. Within $7.6 \mu\text{s}$, during the time elapsed between $195.6 \mu\text{s}$ and $203.2 \mu\text{s}$, the autoignitive front consumes almost all the fresh mixture. An instantaneous peak pressure of approximately 70 atm is reached, consistent with the results reported in [11].

In the next simulation case, we introduce a local hot spot in the initial solution to assess the influence of residual gas in the combustion chamber. The presence of a local hot spot at the initial time is the only difference between the present case and the previously case in Fig. 1. The spatial temperature non-uniformity causes a distribution of local ignition delay time. This induces sequential autoignition events. Results are presented in Fig. 2. At very early time of the calculation (not shown here for better clarity of the figure), as the leading flame propagates the local hot spot is first slowly convected without any noticeable change in magnitudes of pressure or temperature. At a later time, an autoignitive front is triggered from the hot

spot. Subsequently, the autoignitive front strengthens and expands in both directions of the flow, as noticed by the temperature profile at 73 μs . At 82 μs , two detonation waves develop and propagate in the opposite directions of the chamber. The developing detonation towards the right travels at approximately 2100 m/s. A localized overpressure slightly higher than 80 atm and a temperature peak of the order of 3350 K are recorded. These values are higher than those recorded in the case without the initial hot spot. Later on, the detonation waves become sharper and sharper as time evolves. At 86.65 μs , the pressure reaches 100 atm near the right wall.

The influence of the shape of the initial hot spot has been also investigated. Calculations conducted with a temperature elevation of $\Delta T_0 = 10$ K shows globally a developing detonation wave, as previously observed. However, developing detonations are observed in longer time compared to the case where $\Delta T_0 = 100$ K.

4 Conclusions

The present study examined the interaction between a leading flame and a local hot spot in a closed chamber through direct numerical simulations using detailed chemistry. To our best knowledge, this study is one of the first attempts to demonstrate flame-hot-spot interaction in a closed chamber. Our results showed that an autoignitive front, triggered from the local hot spot, expands in the combustion chamber. At early propagation time the autoignitive front is a deflagration. It then accelerates and transits to a detonation mode due to a positive feedback coupling between the pressure pulse and the chemical heat released. The local hot spot distributes the ignition delay time and leads to a detonation development in the combustion chamber. However, the initial temperature gradients used in our investigation show a little influence on the overall transition process.

In internal combustion engine applications, effects of heat losses at walls are important; therefore, additional computations considering wall heat losses need to be investigated. Furthermore, combined effects of temperature and mixture concentration will be investigated in order to represent realistic engine conditions.

Acknowledgments

The work presented in this paper was sponsored by King Abdullah University of Science and Technology and Saudi Aramco under the FUELCOM Program. The computational work utilized the resources at the KAUST Supercomputing Laboratory and Research Computing.

References

- [1] A.E. Lutz, R.J. Kee, J.A. Miller, H.A. Dwyer, A.K. Oppenheim, Dynamic effects of autoignition centers for hydrogen and C1, 2-hydrocarbon fuels, *Proc. Combust. Inst.* 22: 1683–1693 (1988).
- [2] P Dai, Z Chen, S Chen, Y Ju, Numerical experiments on reaction front propagation in n-heptane/air mixture with temperature gradient, *Proceedings of the Combustion Institute* 35 (2015) 3045–3052.
- [3] D. Bradley, G.T. Kalghatgi, Influence of autoignition delay time characteristics of different fuels on pressure waves and knock in reciprocating engines, *Combust. Flame*, 156 (2009), 2307–2318.

- [4] N. Peters, B. Kerschgens, and G. Paczko, Super-Knock Prediction Using a Refined Theory of Turbulence, *SAE Int. J. Engines* 6(2):2013, doi:10.4271/2013-01-1109.
- [5] Ya. B. Zeldovich, Regime classification of an exothermic reaction with nonuniform initial conditions, *Combustion and Flame* 39 (1980) 211-214.
- [6] D. Bradley, 'Hot spots' and gasoline engine knock, *J. Chem. Soc., Faraday Trans.* 92 (1996) 2959-2964.
- [7] D. Bradley, C. Morley, X.J. Gu, Amplified pressure waves during autoignition: relevance to CAI engines, *SAE Paper* 2002-01-2868 (2002).
- [8] X.J. Gu, D.R. Emerson, D. Bradley, Modes of reaction front propagation from hot spots, *Combustion and Flame* 133 (2003) 63-74.
- [9] G.T. Kalghatgi, D. Bradley, Pre-ignition and 'super-knock' in turbo-charged spark-ignition engines, *Int. J. Engine Res.* 13(4) (2012) 399-414.
- [10] L. Bates, D. Bradley, G. Paczko, N. Peters, Engine hot spots: Modes of auto-ignition and reaction propagation, *Combustion and Flame* 166 (2016), 80-85.
- [11] H. Yu, Z. Chen, End-gas auto ignition and detonation development in a closed chamber, *Combustion and Flame* 162 (2015) 4102-4111.
- [12] P. Dai, C. Qi, Z. Chen, Effects of initial temperature on autoignition and detonation development in dimethyl ether/air mixtures with temperature gradient, *Proc. Comb. Inst.* 36 (2017) XXX-XXX.
- [13] C. Qi, P. Dai, H. Yu, Z. Chen, Different modes of reaction front propagation in n-heptane/air mixture with concentration non-uniformity, *Proc. Comb. Inst.* 36 (2017) XXX-XXX.
- [14] CW. Shu, Essentially non-oscillatory and weighted essentially non-oscillatory schemes for hyperbolic conservation laws, *Advanced numerical approximation of nonlinear hyperbolic equations*, (1998), 325-432.
- [15] M.P. Burke, M. Chaos, Y. Ju, F.L. Dryer, S.J. Klippenstein, Comprehensive H₂/O₂ Kinetic Model for High-Pressure Combustion, *Int.J. Chem. Kinet.* (2011).
- [16] D. G. Goodwin, H. K. Moffat, R. L. Speth, Cantera: an object-oriented software toolkit for chemical kinetics, thermodynamics, and transport processes, Version 2.2.1 (2016), <http://www.cantera.org>.
- [17] J.B. Martz, H. Kwak, H.G. Im, G.A. Lavoie, D.N. Assanis, Computational regime of a reacting front propagating into an auto-igniting mixture, *Proc. Comb. Inst.* 33 (2011) 3001-3006.
- [18] J.B. Martz, G.A. Lavoie, H.G. Im, R.J. Middleton, A. Babajimopoulos, D.N. Assanis, The propagation of a laminar reaction front during end-gas auto-ignition, *Combustion and Flame* 159 (2012) 2077-2086.

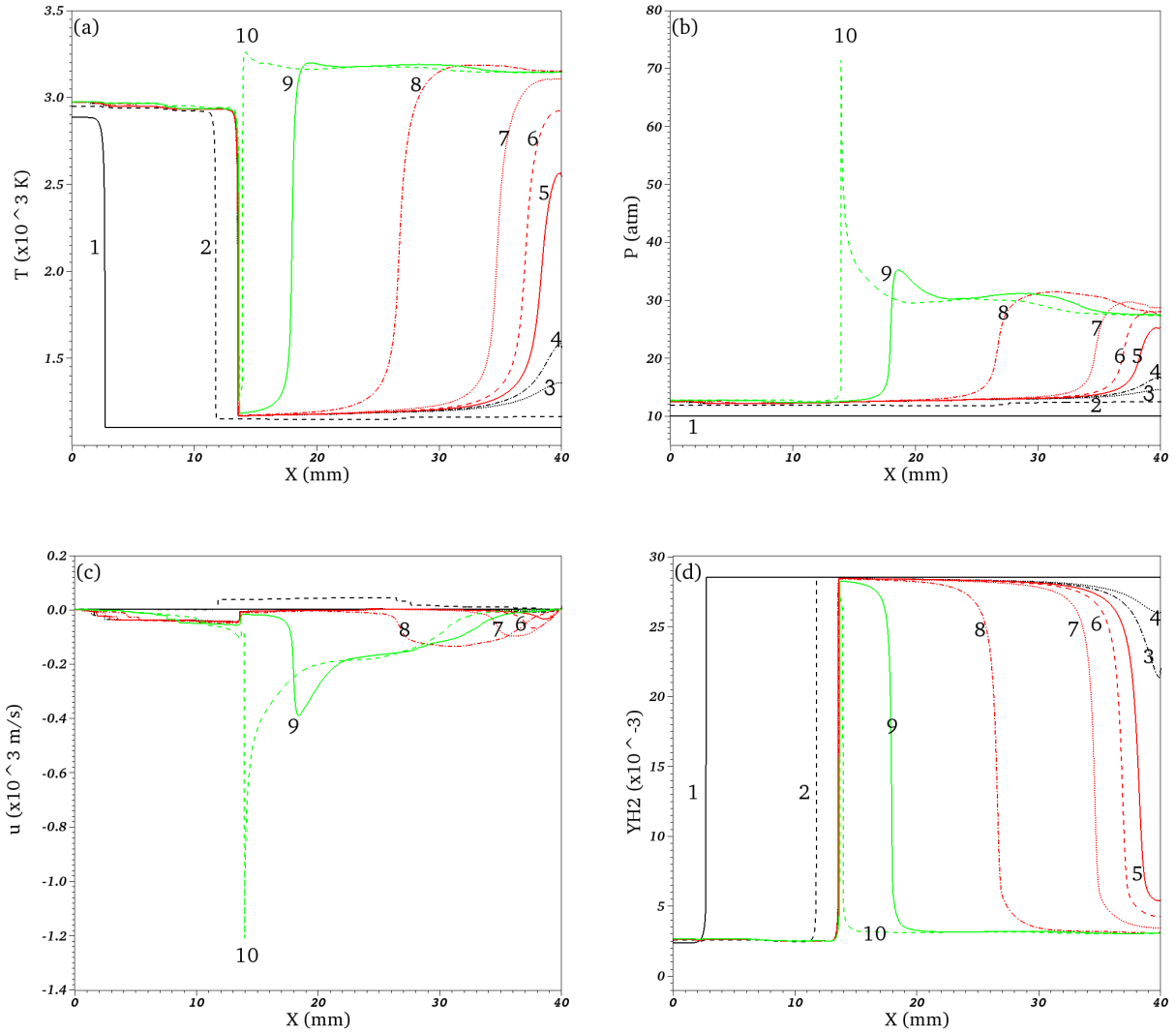


Figure 1: Temporal evolution of temperature, pressure, velocity and H_2 mass fraction distributions. 1– 0 μs , 2– 163.7 μs , 3– 195.4 μs , 4– 195.6 μs , 5– 195.8 μs , 6– 196 μs , 7– 196.4 μs , 8– 198 μs , 9– 201 μs and 10– 203.2 μs .

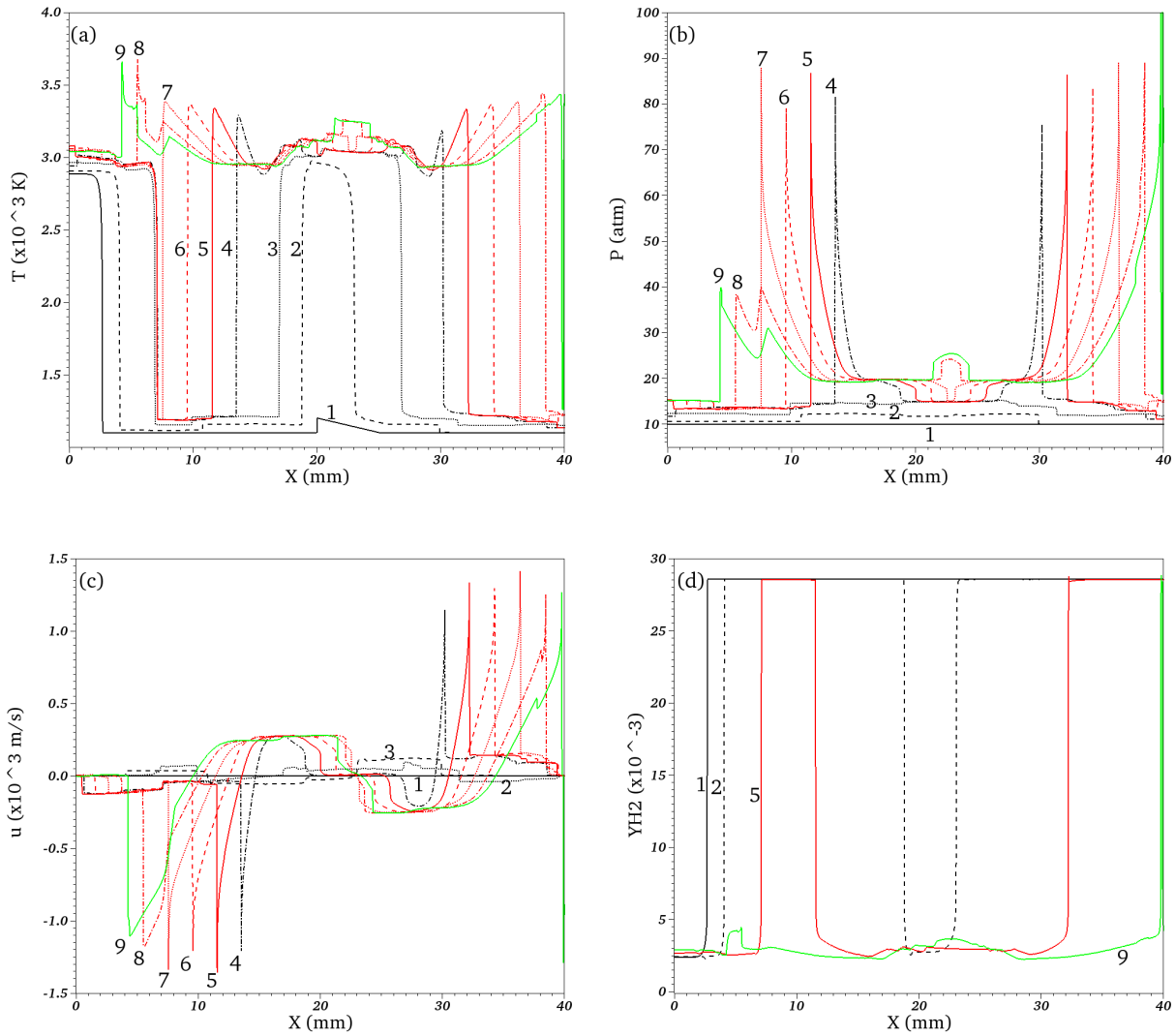


Figure 2: Temporal evolution of temperature, pressure, velocity and H_2 mass fraction distributions. 1– $0 \mu s$, 2– $26 \mu s$, 3– $73 \mu s$, 4– $82 \mu s$, 5– $83 \mu s$, 6– $84 \mu s$, 7– $85 \mu s$, 8– $86.60 \mu s$ and 9– $86.65 \mu s$.